Chemotaxis Assay

The chemotactic activity of THP-1 cells in response to MCP-1 was measured by a Boyden chamber method, as described previously.[30] Additional details can be found in the online-only Data Supplement.

Statistical Analysis

Data are expressed as mean±SE. For analysis of the number of buried/disrupted fibrous caps, differences were analyzed statistically by ANOVA followed by the Dunn multiple comparison test, and differences between 2 groups were analyzed with the Mann-Whitney test. For the other analyses, differences were analyzed statistically by ANOVA followed by post hoc Bonferroni or Dunnett multiple comparison tests. Differences between 2 groups were analyzed with an unpaired *t* test. $P<0.05$ was considered significant.

Results

Adoptive Transfer of Inflammatory Macrophages Accelerated Plaque Destabilization and Rupture

To clarify the role of inflammatory monocyte/macrophages in plaque destabilization and rupture, we first examined whether the adoptive transfer of inflammatory macrophages accelerates plaque destabilization and rupture in a murine model. We collected thioglycollate-induced peritoneal leukocytes from ApoE$^{-/-}$CCR2$^{+/+}$ mice that contained Ly-6C^{high} inflammatory macrophages and from ApoE$^{-/-}$CCR2$^{-/-}$ mice that contained <5% inflammatory macrophages (Figure IIA and IIB in the online-only Data Supplement).[4,31] ApoE$^{-/-}$ mice were assigned to the no-treatment group, the CCR2$^{+/+}$ inflammatory macrophage group (1×10^6 peritoneal leukocytes from ApoE$^{-/-}$CCR2$^{+/+}$ mice), or the CCR2$^{-/-}$ leukocyte group (1×10^6 peritoneal leukocytes from ApoE$^{-/-}$CCR2$^{-/-}$ mice). The adoptive transfer of CCR2$^{+/+}$ inflammatory macrophages tended to increase the incidence of disrupted/buried fibrous caps. The adoptive transfer of CCR2$^{-/-}$ leukocytes significantly decreased the incidence of disrupted/buried fibrous caps compared with that of CCR2$^{+/+}$ inflammatory macrophages (Figure 1A; Table 1). These results demonstrate that inflammatory macrophages responsible for plaque rupture are recruited from the circulation via MCP-1/CCR2 signaling, which suggests a role for peripheral Ly-6C^{high} monocytes as the precursor of inflammatory macrophages. Because splenic monocytes show a phenotype comparable to that of peripheral monocytes,[32] we purified splenic monocytes from ApoE$^{-/-}$ mice fed a high-fat diet and examined whether the adoptive transfer of splenic monocytes accelerated plaque destabilization and rupture in the same model. We confirmed ≈90% purity of splenic monocytes after negative selection using magnetic cell separation, ≈85% of which expressed a high level of Ly-6C (Figure IIIA in the online-only Data Supplement). Consistent with the data from the adoptive transfer of CCR2$^{+/+}$ peritoneal macrophages, the adoptive transfer of splenic monocytes tended to increase the incidence of disrupted/buried fibrous caps ($P=0.056$; Figure IIIB in the online-only Data Supplement), which confirms the detrimental role of inflammatory monocyte/macrophage lineage in atherosclerotic plaque rupture (Figure IIIB in the online-only Data Supplement).

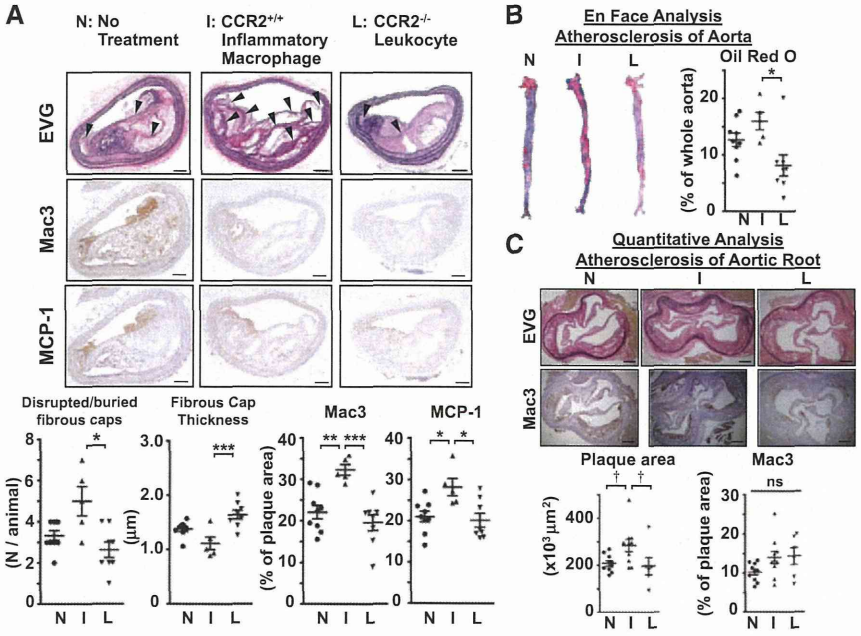

Figure 1. The adoptive transfer of inflammatory macrophages accelerated plaque destabilization and rupture. **A**, **Top**, Photomicrographs of atherosclerotic plaques in the brachiocephalic artery stained with elastica van Gieson (EVG), the antimacrophage surface glycoprotein Mac3, and monocyte chemoattractant protein-1 (MCP-1) in the no-treatment (N), CCR2$^{+/+}$ inflammatory macrophage (I), and CCR2$^{-/-}$ leukocyte (L) groups. Arrowheads indicate disrupted/buried fibrous caps. Scale bar=100 μm. **Bottom**, Quantitation of the number of disrupted/buried fibrous caps, fibrous cap thickness, and Mac3- and MCP-1–positive areas. Data are mean±SEM. *$P<0.05$, **$P<0.01$, and ***$P<0.001$ vs CCR2$^{+/+}$ inflammatory macrophage group. **B**, **Top**, Photomicrographs of the intraluminal surface of the total aorta, stained with oil red O. **Bottom**, Quantitation of the percentage of oil red O–positive area compared with total luminal surface area. Data are mean±SEM. *$P<0.05$ vs CCR2$^{+/+}$ inflammatory macrophage group. **C**, **Top**, Photomicrographs of atherosclerotic plaques in aortic root stained with EVG or Mac3. **Bottom**, Quantitation of plaque size and Mac3-positive areas. Scale bar, 200 μm. Data are mean±SEM. †$P<0.05$ vs CCR2$^{+/+}$ inflammatory macrophage group by 1-way ANOVA followed by Dunnett multiple comparison tests.

Table 1. Characteristics of Brachiocephalic Artery Plaques in the No-Treatment, CCR2$^{+/+}$ Inflammatory Macrophage, and CCR2$^{-/-}$ Leukocyte Groups

	No Treatment (n=9)	CCR2$^{+/+}$ Inflammatory Macrophage (n=5)	CCR2$^{-/-}$ Leukocyte (n=8)
Ruptured plaques per animal, n	3.3±0.2	5.0±0.7†	2.6±0.4
Plaque area, $\times 10^3$ μm^2	230±10	230±10	170±10*
Fibrous cap thickness, μm	1.6±0.2	1.1±0.1†††	2.2±0.3
Lipid core area, %	15±3	20±4	15±3
Macrophage area, %	22±2	32±1**†††	20±3
MCP-1 area, %	21±1	28±2*†	20±3

Data are mean±SEM. Data concerning ruptured plaques per animal were compared by ANOVA followed by Dunn multiple comparison tests. The other data were compared by ANOVA followed by Bonferroni multiple comparison tests. MCP-1 indicates monocyte chemoattractant protein-1.

*P<0.05 vs no-treatment group; **P<0.01 vs no-treatment group;

†P<0.05 vs CCR2$^{-/-}$ leukocyte group; †††P<0.001 vs CCR2$^{-/-}$ leukocyte group.

Immunohistochemical analysis of serial sections revealed that Mac3-positive macrophage infiltration was observed frequently in the shoulder regions of atherosclerotic plaques, and this infiltration was increased in the CCR2$^{+/+}$ inflammatory peritoneal macrophage group compared with the no-treatment group (Figure 1A; Table 1). MCP-1 immunostaining colocalized with macrophages and was also observed in the media. MCP-1 expression in atherosclerotic plaques increased in the CCR2$^{+/+}$ inflammatory macrophage group compared with the no-treatment group, but not in the CCR2$^{-/-}$ leukocyte group (Figure 1A; Table 1). In a subset of experiments, we labeled peritoneal macrophages with PKH26 before adoptive transfer and found that PKH26-labeled peritoneal macrophages were present in the atherosclerotic plaques in the brachiocephalic arteries (Figure IIC in the online-only Data Supplement). In the whole aorta and aortic root, the adoptive transfer of CCR2$^{+/+}$ inflammatory macrophages increased the atherosclerosis area compared with the adoptive transfer of CCR2$^{-/-}$ leukocytes (Figure 1B and 1C), although the serum lipid profile was comparable among the 3 groups (Table I in the online-only Data Supplement).

Measurement of serum biomarkers with a multiplex immunoassay system showed that the adoptive transfer of CCR2$^{+/+}$ peritoneal macrophages, but not CCR2$^{-/-}$ leukocytes, increased the serum levels of MCP-1, MCP-3, and MCP-5, as well as monocyte colony-stimulating factor (Table II in the online-only Data Supplement). Importantly, the adoptive transfer of CCR2$^{+/+}$ inflammatory macrophages increased MMP-9, a metalloproteinase that may degrade the fibrous cap of plaques. Interestingly, the adoptive transfer of CCR2$^{+/+}$ inflammatory macrophages did not affect the serum levels of inflammatory cytokines, such as interferon-γ, tumor necrosis factor-α, and the interleukin family (Table II in the online-only Data Supplement).

Cellular Uptake and In Vitro Kinetics of PLGA Nanoparticles in Macrophages

To clarify the advantage of the nanoparticle-mediated DDS for targeting inflammatory monocytes/macrophages, the cellular uptake and kinetics of PLGA nanoparticles were examined in cultured macrophages. Murine peritoneal macrophages took up FITC-NPs, which were distributed within the cytosol, as detected by confocal microscopy (Figure IVA and IVB in the online-only Data Supplement). Electron microscopy revealed that the PLGA nanoparticles were incorporated into the lysosomes (Figure IVC in the online-only Data Supplement). Cellular uptake of FITC-NP and FITC was quantified as the cellular fluorescent intensity in RAW264.7 cells after a 2-hour incubation with FITC-NP or FITC, followed by a washout period. The FITC signal intensity in cells incubated with FITC-NPs was greater than in cells incubated with FITC over a 7-day period (Figure IVD in the online-only Data Supplement), which suggests that FITC-NP leads to enhanced and sustained uptake in cultured macrophages.

In Vivo Localization of FITC-NPs After Intravenous Administration

Flow cytometric analysis of the blood revealed that neutrophils (36±13%) and monocytes (61±13%) had an FITC signal 2 hours after FITC-NP injection, which suggests that FITC-NPs were taken up through phagocytosis. Flow cytometric analysis of the spleen also revealed the uptake of FITC-NPs in neutrophils and monocytes (Figure 2A). Fluorescence microscopy analysis of the aortic arch and the brachiocephalic arteries revealed the presence of FITC signals mainly in the macrophage areas of atherosclerotic plaques in FITC-NP–injected animals (Figure 2B).

Treatment With Pitavastatin-NPs Inhibits Plaque Destabilization and Rupture

A 4-week treatment with pitavastatin-NPs, but not with FITC-NPs or pitavastatin, significantly reduced the incidence of disrupted/buried fibrous caps associated with thick luminal fibrous caps (Figure 3A; Table 2) and decreased serum biomarkers, including MCP-1, CD40L, vascular endothelial growth factor, and von Willebrand factor (Table III in the online-only Data Supplement). To clarify the pharmacokinetics of nanoparticle treatment, we measured plasma concentration of pitavastatin in the pitavastatin and pitavastatin-NP groups. Plasma concentration of pitavastatin was below the limit of detection (0.625 ng/mL) except 2 hours after intravenous injection of pitavastatin-NP (Table IV in the online-only Data Supplement). There were no significant differences in lipid profiles among the 4 groups (Table V in the online-only Data Supplement). Immunohistochemical analysis revealed that treatment with pitavastatin-NPs attenuated the infiltration of Mac3-positive cells and MCP-1 expression in atherosclerotic plaques (Figure 3A; Table 2). In cultured monocytes, pretreatment with pitavastatin-NPs at 10 μmol/L, but not with pitavastatin at the same dose, inhibited interferon-γ–induced gene expression of MCP-1 (Figure 4B). Consistent with these data, treatment with pitavastatin-NPs, but not FITC-NPs or pitavastatin, decreased the atherosclerosis area in the whole aorta and aortic root (Figure 3B and 3C). Treatment with pitavastatin-NPs, but not with FITC-NPs or pitavastatin, also attenuated the infiltration of Mac3-positive cells to the aortic root (Figure 3C).

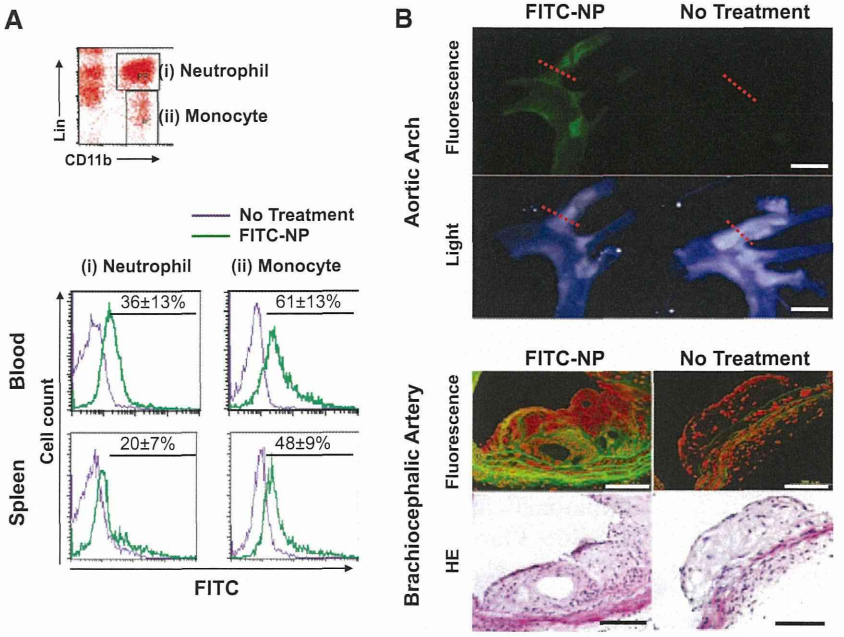

Figure 2. In vivo nanoparticle-mediated drug delivery. **A**, Representative flow cytometry dot plots of circulating leukocytes 2 hours after intravenous injection of PLGA nanoparticles encapsulated with FITC (FITC-NP). Cells were stained with lineage markers and anti-CD11b. The histograms demonstrate FITC uptake by neutrophils (i) and monocytes (ii) in the blood and spleen. Purple indicates control fluorescence in cells derived from uninjected mice. Green indicates fluorescence in cells derived from FITC-NP–injected mice. The percentages of FITC-positive cells is reported as mean±SEM (n=3 per group). **B, Top**, Representative fluorescent and light stereomicrographs of isolated segments of the aortic arch 24 hours after intravenous injection of saline (control) or FITC-NPs. Scale bar, 1 mm. **Bottom**, Representative photomicrographs of serial sections of atherosclerotic plaques in the brachiocephalic artery (red dotted line of upper panel) examined with fluorescence microscopy or stained with hematoxylin-eosin (HE). In the fluorescent micrographs, the nuclei were counterstained with propidium iodide (red). Scale bar, 200 μm.

Treatment With Pitavastatin-NPs Inhibits Gelatinase Activity in the Atherosclerotic Plaque

As reported previously, MMP secretion was upregulated in inflammatory monocytes, and focal activation of MMPs is another potential mechanism through which plaques can be destabilized.[33] In situ zymography revealed that pitavastatin-NPs but not control nanoparticles reduced gelatinase activity (Figure 5A). A gelatinase activity

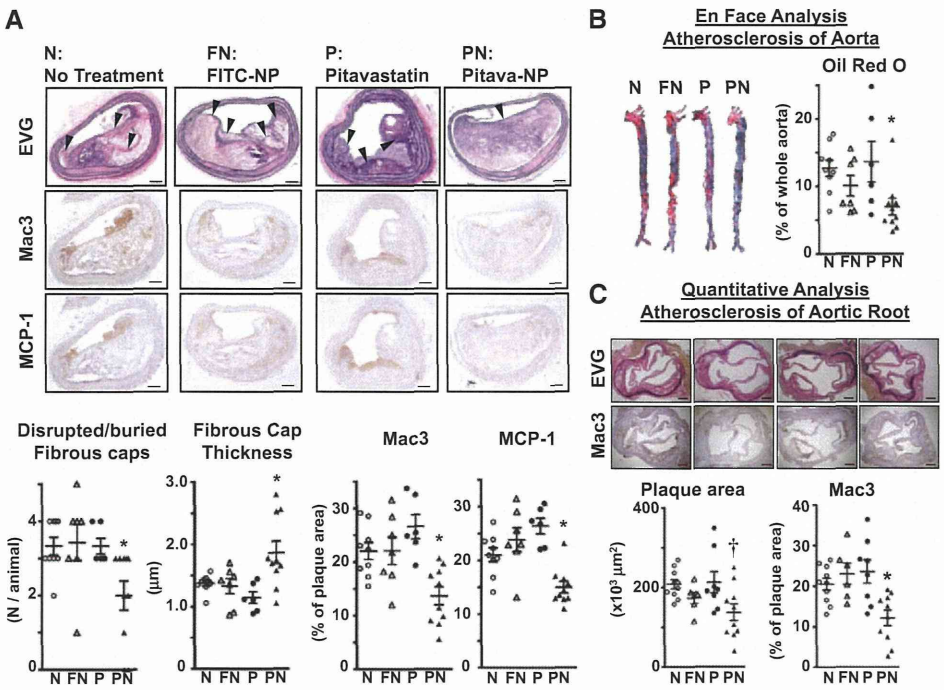

Figure 3. Treatment with nanoparticles (NPs) encapsulated with pitavastatin (Pitava-NP) inhibits atherosclerotic plaque destabilization and rupture. **A, Top**, Photomicrographs of atherosclerotic plaques in the brachiocephalic artery stained with elastica van Gieson (EVG), the antimacrophage surface glycoprotein Mac3, and monocyte chemoattractant protein-1 (MCP-1) from the no-treatment (N), FITC-NP (FN), pitavastatin (P), and Pitava-NP groups (PN). Scale bar, 100 μm. **Bottom**, Quantitation of the number of disrupted/buried fibrous caps, fibrous cap thickness, and Mac3- and MCP-1–positive areas. Data are mean±SEM. *P<0.05 vs no-treatment group. **B, Top**, Photomicrographs of intraluminal surface of total aorta stained with oil red O. **Bottom**, Quantitation of percentage of oil red O–positive area compared with total luminal surface area. Data are mean±SEM. *P<0.05 vs no-treatment group. **C, Top**, Photomicrographs of atherosclerotic plaques in aortic root stained with EVG or Mac3. **Bottom**, Quantitation of plaque size and Mac3-positive areas. Scale bar, 200 μm. Data are mean±SEM. †P<0.05 vs no-treatment group by 1-way ANOVA followed by Dunnett multiple comparison tests. *P<0.05 vs no-treatment group by 1-way ANOVA followed by Bonferroni multiple comparison tests.

Table 2. Characteristics of Brachiocephalic Artery Plaques in the No-Treatment, FITC-NP, Pitavastatin, and Pitavastatin-NP Groups

	No Treatment (n=9)	FITC-NP (n=7)	Pitavastatin (n=6)	Pitavastatin-NP (n=10)
Ruptured plaques per animal, n	3.3±0.2	3.4±0.5	3.3±0.2	2.0±0.4*
Plaque area, $\times 10^3$ μm^2	230±10	170±10	130±40*	150±20*
Fibrous cap thickness, μm	1.6±0.2	1.3±0.1	1.2±0.1	1.9±0.2*
Lipid core area, %	15±3	12±3	8±2	11±2
Macrophage area, %	22±2	22±3	27±2	14±3*
MCP-1 area, %	21±1	24±2	26±2	15±3*

Data are mean±SEM. Data concerning ruptured plaques per animal were compared by ANOVA followed by Dunn multiple comparison tests. Other data were compared by ANOVA followed by Bonferroni multiple comparison tests. MCP-1 indicates monocyte chemoattractant protein-1; and NP, nanoparticles.

*P<0.05 vs no-treatment group.

assay with gelatin zymography in the culture medium of RAW264.7 cells showed that pitavastatin-NPs reduced MMP-9 secretion in a dose-dependent manner, whereas the same dose of pitavastatin showed no effects on MMP-9 secretion (Figure 5B). Both the pro-form and active form of MMP-2 were almost undetectable in the culture medium of RAW264.7 cells, even when stimulated with lipopolysaccharide (Figure 5B).

Treatment With Pitavastatin-NPs Inhibits the Recruitment of Ly-6C^{high} Monocytes to the Circulating Blood

Monocytosis and increased Ly-6C^{high} monocytes in the circulating blood critically promote the progression of atherosclerosis.[31] Treatment with pitavastatin-NP reduced the percentage of monocytes among the total leukocytes on days 7 (Figure 4A). A monocyte subset analysis showed a marked reduction of Ly-6C^{high} monocytes in the circulating blood in the pitavastatin-NP group (Figure 4A). Although CCR2, a key chemokine receptor that promotes the migration of Ly-6C^{high} monocytes, was not affected by pretreatment with pitavastatin-NPs (Figure 4B), MCP-1–induced chemotaxis was inhibited by pretreatment with pitavastatin-NPs in a dose-dependent manner (Figure 4C).

Nanoparticle-Mediated Anti–MCP-1 Gene Therapy Inhibits Plaque Destabilization and Rupture

To further elucidate the impact of inhibition of MCP-1/CCR2 signaling through a nanoparticle-mediated DDS on plaque destabilization and rupture, we examined the effects of nanoparticles that contained plasmids that encode 7ND, a deletion mutant of MCP-1. We previously reported that systemic gene therapy with the 7ND plasmid attenuated the development and progression of atherosclerosis in ApoE$^{-/-}$ mice[27,34–36] and that nanoparticle-mediated transfection of the 7ND plasmid inhibited MCP-1–induced monocyte chemotaxis ex vivo.[37] Treatment with 7ND-NPs reduced macrophage infiltration into the plaques and the incidence of disrupted/buried fibrous caps associated with thick fibrous caps (Figure 6A;

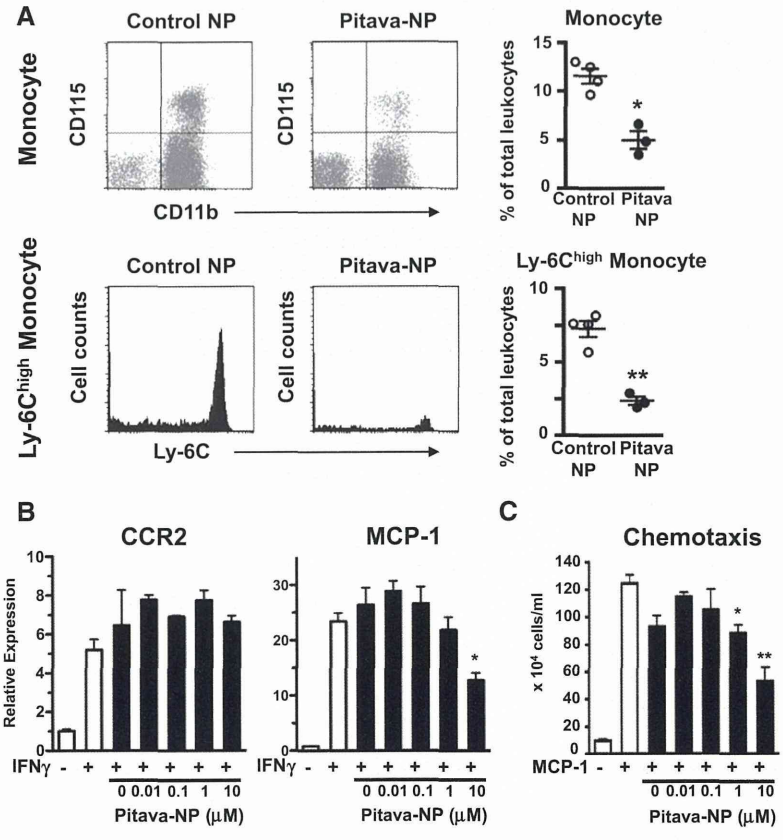

Figure 4. Effects of nanoparticles (NPs) encapsulated with pitavastatin (Pitava-NP) on recruitment of Ly-6C^{high} monocytes. **A, Left,** Representative flow cytometry dot plots and histograms from mice injected intravenously with control (empty) NPs or pitavastatin-NPs. **Right,** Quantitative analysis of ratio of monocytes and Ly-6C^{high} monocytes to total leukocytes is also presented. Data are mean±SEM (n=3–4 per group). *P<0.005 and **P<0.001 vs Control-NP group by unpaired t test. **B,** Effects of pitavastatin-NPs on mRNA levels of CCR2 and monocyte chemoattractant protein-1 (MCP-1) in RAW264.7 cells. Data are mean±SEM (n=3 per group). Data were compared by 1-way ANOVA followed by Bonferroni multiple comparison tests. *P<0.05 vs interferon-γ (IFNγ) group. **C,** Effects of pitavastatin-NPs on MCP-1–induced monocyte chemotaxis in THP-1 cells. Data are mean±SEM (n=3 per group). Data were compared by 1-way ANOVA followed by Bonferroni multiple comparison tests. *P<0.05 and **P<0.001 vs MCP-1 group.

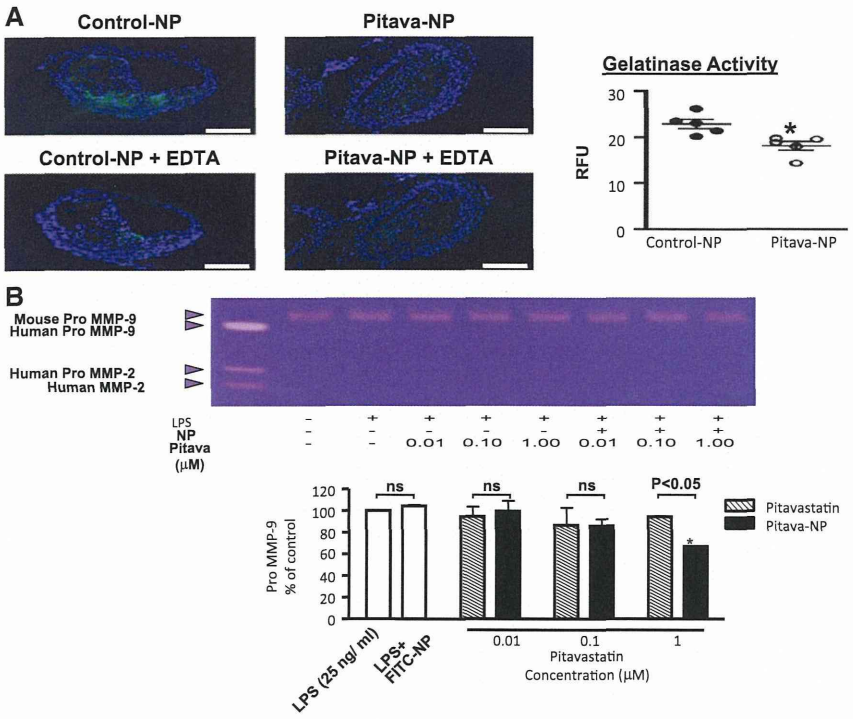

Figure 5. Effects of nanoparticles (NPs) encapsulated with pitavastatin (Pitava-NP) on gelatinase activity of atherosclerotic plaque. **A, Left,** In situ zymography for gelatinase activity of atherosclerotic plaque in brachiocephalic artery. Nuclei were counterstained with DAPI. Scale bar, 100 μm. The addition of EDTA was used as a negative control for each section. **Right,** Quantitative analysis of relative fluorescence units (RFUs) of gelatinase activity in atherosclerotic plaques treated with control NPs or pitavastatin-NPs. Data are mean±SEM. *P<0.05 vs Control-NP group by unpaired t test. **B,** Quantitative analysis of native form of matrix metalloproteinase-9 (MMP-9) by gelatin zymography. Data are mean±SEM (n=3 per group) and were compared by 2-way ANOVA followed by Bonferroni multiple comparison tests. *P<0.05 vs lipopolysaccharide (LPS) group by 1-way ANOVA followed by Bonferroni multiple comparison tests.

Table 3), although the serum lipid profile was comparable (Table VI in the online-only Data Supplement). In contrast, treatment with 7ND-NPs did not decrease the atherosclerosis area in the aorta (Figure 6B).

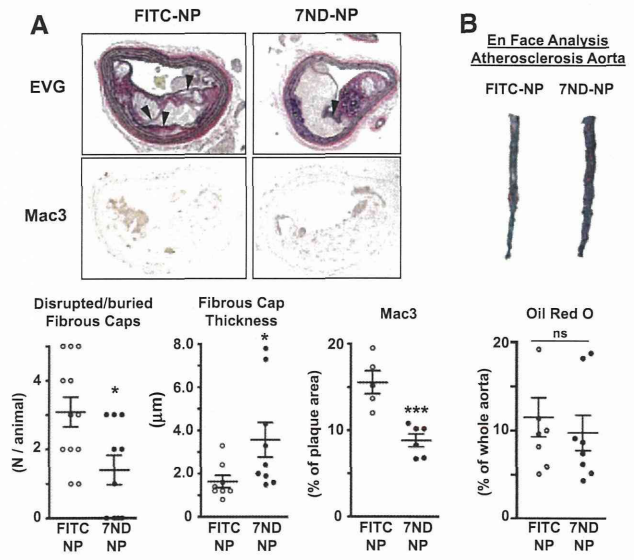

Figure 6. Nanoparticle-mediated anti–MCP-1 (monocyte chemoattractant protein-1) gene therapy inhibits plaque destabilization and rupture. **A, Top,** Photomicrographs of atherosclerotic plaques in brachiocephalic artery stained with elastica van Gieson (EVG) or Mac3. Arrowheads indicate disrupted/buried fibrous caps. Scale bar, 100 μm. **Bottom,** Quantitative comparison of number of disrupted/buried fibrous caps, fibrous cap thickness, and Mac3-positive area. Data are mean±SEM. *P<0.05 and ***P<0.001 vs FITC-NP group. **B,** Quantitation of percentage of plaque area compared with total luminal surface area. Data are mean±SEM. There were no statistically significant differences between the 2 groups. FITC-NP indicates nanoparticles encapsulated with FITC, 7ND-NP, nanoparticles encapsulated with 7ND plasmid.

Effects of Oral Treatment With Pitavastatin on Plaque Destabilization and Rupture

Daily oral administration of pitavastatin 0.1 mg/kg had no significant effects on plaque destabilization and rupture, but administration of pitavastatin at 1.0 mg/kg reduced the incidence of disrupted/buried fibrous caps associated with thick fibrous caps and plaque size (Figure VA in the online-only Data Supplement; Table 4). Daily oral administration of pitavastatin 1.0 mg/kg also decreased the atherosclerosis area in the whole aorta and aortic root, whereas administration of pitavastatin 0.1 mg/kg did not (Figure VB and VC in the online-only Data Supplement). Daily oral administration of pitavastatin 1.0 mg/kg significantly inhibited macrophage infiltration and MCP-1 expression in the brachiocephalic artery (Mac3 immunostaining area: 49±3 [$\times 10^3$ μm^2; n=9], 53±5 [$\times 10^3$ μm^2; n=10], and 22±4 [$\times 10^3$ μm^2; n=11] for no treatment, pitavastatin 0.1 mg/kg, and pitavastatin 1 mg/kg, respectively; P<0.01 for no treatment versus pitavastatin 1 mg/kg; MCP-1 immunostaining area: 47±3 [$\times 10^3$ μm^2; n=9],

Table 3. Characteristics of Brachiocephalic Artery Plaques in the FITC-NP and 7ND-NP Groups

	FITC-NP	7ND-NP
Ruptured plaques per animal, n	3.1±0.4 (n=12)	1.4±0.4* (n=10)
Plaque area, $\times 10^3$ μm^2	140±15 (n=8)	170±30 (n=5)
Fibrous cap thickness, μm	1.6±0.3 (n=8)	3.6±0.8* (n=9)
Macrophage area, %	16±1 (n=5)	9±1* (n=6)
MCP-1 area, %	17±2 (n=6)	14±3 (n=6)

Data are mean±SEM. Data concerning ruptured plaques per animal were compared by Mann-Whitney test. Other data were compared by unpaired t test.
MCP-1 indicates monocyte chemoattractant protein-1; and NP, nanoparticles.
*P<0.05 vs FITC-NP.

Table 4. Characteristics of Brachiocephalic Artery Plaques in the No-Treatment, Pitavastatin 0.1 mg/kg, and Pitavastatin 1.0 mg/kg Groups

	No Treatment (n=9)	Pitavastatin 0.1 mg/kg (n=10)	Pitavastatin 1.0 mg/kg (n=11)
Ruptured plaques per animal, n	3.3±0.2	3.2±0.7	1.9±0.3†
Plaque area, $\times 10^3$ μm^2	230±10	190±20	130±10*
Fibrous cap thickness, μm	1.6±0.2	1.5±0.1	2.6±0.4**
Lipid core area, %	15±3	26±2	14±2
Macrophage area, %	22±2	26±3	18±4
MCP-1 area, %	21±1	17±1	16±3

Data are mean±SEM. Data concerning ruptured plaques per animal were compared by ANOVA followed by Dunn multiple comparison tests. Other data were compared by ANOVA followed by Bonferroni multiple comparison tests. MCP-1 indicates monocyte chemoattractant protein-1.

*$P<0.05$ vs the no-treatment group; **$P<0.01$ vs the no-treatment group.

†$P<0.05$ vs the no-treatment group; data were compared by ANOVA followed by Dunnett multiple comparison tests.

40±5 [$\times 10^3$ μm^2; n=10], and 21±2 [$\times 10^3$ μm^2; n=11] for no treatment, pitavastatin 0.1 mg/kg, and pitavastatin 1 mg/kg, respectively; $P<0.01$ for no treatment versus pitavastatin 1 mg/kg; Figure VA in the online-only Data Supplement; Table 4). The serum lipid profile was comparable among the 3 groups (Table VII in the online-only Data Supplement). The cumulative effective dose of orally administered pitavastatin was ≈20 times greater than that of the dose of pitavastatin-NPs required to achieve plaque stability (28 versus 1.6 mg/kg, respectively).

Discussion

Advanced atherosclerotic plaques spontaneously rupture in the brachiocephalic arteries of ApoE$^{-/-}$ or low-density lipoprotein receptor–deficient (LDL-R$^{-/-}$) mice, and this rupture appears to represent several key histological features of ruptured human plaques, including an increase in plaque destabilization markers (eg, monocyte infiltration/activation, lipid accumulation, fibrous cap thinning) and evidence of disrupted and buried fibrous caps.[17,33,38,39] The recruitment of Ly-6C^{high} monocytes was observed during the development of aortic atherosclerosis in ApoE$^{-/-}$ mouse[31]; however, substantial proof for a decisive role of Ly-6C^{high} monocytes in plaque destabilization and rupture has been lacking. In the present study, we used this murine model and found that (1) the recruitment of inflammatory monocytes into the atherosclerotic plaque is critical for accelerating plaque destabilization and (2) the nanoparticle-mediated delivery of pitavastatin inhibits plaque destabilization and rupture by inhibiting the recruitment of inflammatory monocytes.

A recent study reported that local macrophage proliferation rather than monocyte recruitment is a major component of atherosclerosis formation.[40] In the present study, we demonstrated that the adoptive transfer of inflammatory monocytes accelerated plaque destabilization in a CCR2-dependent manner, which suggests a role of direct recruitment of inflammatory monocytes in this process. The different importance of monocyte recruitment and local macrophage proliferation between these studies may be attributable to the difference in the model, because angiotensin II infusion strongly induces MCP-1 expression in arterial walls,[41] which might reveal the importance of monocyte recruitment. There is a possibility that adoptive transfer of inflammatory monocytes indirectly enhanced local macrophage proliferation through an increase in serum monocyte-colony stimulating factor (Table II in the online-only Data Supplement) to accelerate atherosclerosis. Further study is needed to examine the relative importance of different mechanisms of monocyte/macrophage contribution to atherosclerosis in different pathological settings. Adoptive transfer of CCR2$^+$Ly-6C^{high} macrophages also increased serum levels of monocyte/macrophage chemoattractants (MCP-1, MCP-3, and MCP-5; Table II in the online-only Data Supplement), which might further accelerate monocyte/macrophage-mediated inflammation. These findings suggest that targeting CCR2$^+$Ly-6C^{high} inflammatory monocytes/macrophages with a DDS is a promising strategy to inhibit the destabilization of rupture-prone atherosclerotic plaques.

We used a PLGA nanoparticle as a phagocyte-directed DDS in the present study because PLGA is a biocompatible material that is already in clinical use. Intravenously administered FITC-NPs were rapidly taken up by circulating and splenic leukocytes, predominantly by monocytes/macrophages, and accumulated in macrophages in atherosclerotic plaques (Figure 2). An in vitro pharmacodynamics assay with FITC-NPs showed that nanoparticulation enhanced cellular uptake and retention over a 7-day period in cultured macrophages (Figure IV in the online-only Data Supplement). Weekly intravenous treatment with pitavastatin-NPs inhibited plaque destabilization and rupture associated with reduced macrophage infiltration and MCP-1 expression without affecting serum cholesterol levels. We previously reported that pitavastatin-NPs inhibited lipopolysaccharide-induced nuclear factor-κB activation in cultured macrophages.[24] Nuclear factor-κB is a central regulator of monocyte inflammatory activation and leads to the upregulation of MCP-1 and MMP expression.[42] Indeed, pitavastatin-NPs inhibited MCP-1 expression and gelatinase activity in macrophages both in vivo and in vitro. In the present study, interference with MCP-1/CCR2 signaling by the intravenous administration of 7ND-NP inhibited the recruitment of monocytes into the plaque, followed by plaque stabilization in the brachiocephalic artery (Figure 6), which confirms the pivotal role of MCP-1/CCR2 signaling–mediated monocyte migration, which makes this signaling pathway a therapeutic target to inhibit plaque destabilization. In the present study, aortic atherosclerosis was not reduced by intravenous injection of 7ND-NPs, which primarily target circulating monocytes and their microenvironment.[37] We have reported previously that aortic atherosclerosis in ApoE$^{-/-}$ mice fed a high-fat diet (without angiotensin II infusion) was attenuated by HVJ (hemagglutinating virus of Japan; Sendai virus) liposome–mediated 7ND gene transfer into hindlimb muscles, which maintains 7ND-mutant MCP-1 in the circulation.[34] Because we have previously shown that angiotensin II infusion strongly induces MCP-1 expression in smooth muscle cells in the aorta,[41] a different source of MCP-1 (macrophages in the setting of a high-fat

diet, and macrophages and smooth muscle cells in the setting of a high-fat diet and angiotensin II infusion) might affect the different therapeutic effect of 7ND plasmid on a different mode of administration, although this was beyond the scope of the present study.

Importantly, pitavastatin-NPs reduced the number of circulating Ly-6C^{high} inflammatory monocytes, which suggests that pitavastatin-NPs inhibited recruitment of Ly-6C^{high} monocytes from the sites of hematopoiesis to the circulation,[43] in addition to inhibiting recruitment from the circulation to the atherosclerotic lesions. Because pitavastatin-NPs did not affect CCR2 expression, in contrast with MCP-1 expression (Figure 4B), pitavastatin-NPs might inhibit monocyte chemotaxis by inhibiting the geranylgeranylation of RhoA, which regulates the ERM (ezrin/radixin/moesin) family of proteins.[44,45]

Pitavastatin was used in the present study because we previously found that this compound elicited the most potent inhibitory effects on HMG-CoA reductase activity in rodent liver microsomes compared with other statins (April, 2012). A prior study reported that daily oral administration of pitavastatin at 1 and 10 mg/kg, which exceeds the clinical norm and could lead to serious adverse side effects, attenuates the development of aortic atherosclerosis in ApoE$^{-/-}$ mice.[46] We thus examined whether nanoparticle-mediated pitavastatin delivery is superior to daily oral administration of pitavastatin alone for the inhibition of aortic atherosclerosis and plaque destabilization and rupture, and we found that oral daily administration of pitavastatin at 0.1 mg·kg^{-1}·d^{-1} for 28 days (cumulative dose, 0.1 mg/body) had no therapeutic effects, but administration of pitavastatin at 1.0 mg·kg^{-1}·d^{-1} (cumulative dose, 1.0 mg/body) showed significant therapeutic effects. Therefore, our nanoparticle-mediated DDS (0.05 mg of pitavastatin per body) potentiated the therapeutic efficacy of pitavastatin (by ≥20-fold). Our nanoparticle-mediated DDS may extend the usages of statin treatment while reducing potential side effects.

There are some limitations in the present study. First, we could not detect thrombus formation in the brachiocephalic artery or myocardial infarction or stroke in our murine model because mouse ruptured plaques rarely undergo thrombotic occlusion, which may reflect the difference in coagulation/fibrinolytic activity between mice and humans.[47]

Second, we could not determine the proportion of transferred macrophages that migrated into the arteries. Although a substantial proportion of transferred macrophages might be trapped in the reticuloendothelial system, such as liver and lung, we did observe increased macrophage infiltration to the brachiocephalic artery associated with upregulated monocyte/macrophage-associated serum proteins, which suggests that transferred macrophages were biologically active in the present study.

Third, the tissue concentrations of pitavastatin could not be measured because the sample size from the brachiocephalic arteries was too small for high-performance liquid chromatography. Although we examined the plasma level of pitavastatin in the pitavastatin and pitavastatin-NP groups, the concentration of pitavastatin could be measured only >2 hours after intravenous injection. Further studies are needed to clarify the in vivo pharmacokinetics of pitavastatin after pitavastatin-NP treatment in larger animals.

Finally, we only adopted the protocol of weekly intravenous administration of pitavastatin-NPs at the indicated dose. The dose of pitavastatin-NPs used in the present study was selected because of its effectiveness in previous studies from our laboratory in murine and rabbit models of hindlimb ischemia.[22,23] Further studies are needed to determine the optimal dose range and interval of pitavastatin-NPs for clinical application.

In conclusion, recruitment of inflammatory monocytes is critical in the pathogenesis of plaque destabilization and rupture. Nanoparticle-mediated pitavastatin delivery inhibited plaque destabilization and rupture and regulated the recruitment of inflammatory monocytes by interfering in MCP-1/CCR2 signaling in this model. This nanotechnology-based modality can be developed as a new therapeutic strategy for vulnerable patients with rupture-prone unstable plaques.

Acknowledgments

We thank Dr Junji Kishimoto for his helpful statistical advice.

Sources of Funding

This study was supported by grants-in-aid for scientific research (22390160, 23790863, and 23790861) from the Ministry of Education, Science, and Culture, Tokyo, Japan, and by health science research grants (research on translational research and nanomedicine) from the Ministry of Health Labor and Welfare, Tokyo, Japan.

Disclosures

Dr Egashira holds a patent on the results reported in the present study. The other authors report no conflicts.

References

1. Go AS, Mozaffarian D, Roger VL, Benjamin EJ, Berry JD, Borden WB, Bravata DM, Dai S, Ford ES, Fox CS, Franco S, Fullerton HJ, Gillespie C, Hailpern SM, Heit JA, Howard VJ, Huffman MD, Kissela BM, Kittner SJ, Lackland DT, Lichtman JH, Lisabeth LD, Magid D, Marcus GM, Marelli A, Matchar DB, McGuire DK, Mohler ER, Moy CS, Mussolino ME, Nichol G, Paynter NP, Schreiner PJ, Sorlie PD, Stein J, Turan TN, Virani SS, Wong ND, Woo D, Turner MB; American Heart Association Statistics Committee and Stroke Statistics Subcommittee. Heart disease and stroke statistics–2013 update: a report from the American Heart Association. *Circulation*. 2013;127:e6–e245.
2. Nahrendorf M, Pittet MJ, Swirski FK. Monocytes: protagonists of infarct inflammation and repair after myocardial infarction. *Circulation*. 2010;121:2437–2445.
3. Hansson GK. Inflammation, atherosclerosis, and coronary artery disease. *N Engl J Med*. 2005;352:1685–1695.
4. Gordon S. Macrophage heterogeneity and tissue lipids. *J Clinical Invest*. 2007;117:89–93.
5. Tsujioka H, Imanishi T, Ikejima H, Kuroi A, Takarada S, Tanimoto T, Kitabata H, Okochi K, Arita Y, Ishibashi K, Komukai K, Kataiwa H, Nakamura N, Hirata K, Tanaka A, Akasaka T. Impact of heterogeneity of human peripheral blood monocyte subsets on myocardial salvage in patients with primary acute myocardial infarction. *J Am Coll Cardiol*. 2009;54:130–138.
6. Shepherd J, Cobbe SM, Ford I, Isles CG, Lorimer AR, MacFarlane PW, McKillop JH, Packard CJ; West of Scotland Coronary Prevention Study Group. Prevention of coronary heart disease with pravastatin in men with hypercholesterolemia. *N Engl J Med*. 1995;333:1301–1307.
7. Downs JR, Clearfield M, Weis S, Whitney E, Shapiro DR, Beere PA, Langendorfer A, Stein EA, Kruyer W, Gotto AM Jr. Primary prevention of acute coronary events with lovastatin in men and women with average cholesterol levels: results of AFCAPS/TexCAPS: Air Force/Texas Coronary Atherosclerosis Prevention Study. *JAMA*. 1998;279:1615–1622.

8. Randomised trial of cholesterol lowering in 4444 patients with coronary heart disease: the Scandinavian Simvastatin Survival Study (4S). *Lancet*. 1994;344:1383–1389.
9. Sacks FM, Pfeffer MA, Moye LA, Rouleau JL, Rutherford JD, Cole TG, Brown L, Warnica JW, Arnold JM, Wun CC, Davis BR, Braunwald E; Cholesterol and Recurrent Events Trial Investigators. The effect of pravastatin on coronary events after myocardial infarction in patients with average cholesterol levels. *N Engl J Med*. 1996;335:1001–1009.
10. Cannon CP, Braunwald E, McCabe CH, Rader DJ, Rouleau JL, Belder R, Joyal SV, Hill KA, Pfeffer MA, Skene AM; Pravastatin or Atorvastatin Evaluation and Infection Therapy-Thrombolysis in Myocardial Infarction 22 Investigators. Intensive versus moderate lipid lowering with statins after acute coronary syndromes. *N Engl J Med*. 2004;350:1495–1504.
11. Nissen SE, Tuzcu EM, Schoenhagen P, Crowe T, Sasiela WJ, Tsai J, Orazem J, Magorien RD, O'Shaughnessy C, Ganz P; Reversal of Atherosclerosis with Aggressive Lipid Lowering (REVERSAL) Investigators. Statin therapy, LDL cholesterol, C-reactive protein, and coronary artery disease. *N Engl J Med*. 2005;352:29–38.
12. Nicholls SJ, Ballantyne CM, Barter PJ, Chapman MJ, Erbel RM, Libby P, Raichlen JS, Uno K, Borgman M, Wolski K, Nissen SE. Effect of two intensive statin regimens on progression of coronary disease. *N Engl J Med*. 2011;365:2078–2087.
13. Patti G, Cannon CP, Murphy SA, Mega S, Pasceri V, Briguori C, Colombo A, Yun KH, Jeong MH, Kim JS, Choi D, Bozbas H, Kinoshita M, Fukuda K, Jia XW, Hara H, Cay S, Di Sciascio G. Clinical benefit of statin pretreatment in patients undergoing percutaneous coronary intervention: a collaborative patient-level meta-analysis of 13 randomized studies. *Circulation*. 2011;123:1622–1632.
14. Aikawa M, Rabkin E, Sugiyama S, Voglic SJ, Fukumoto Y, Furukawa Y, Shiomi M, Schoen FJ, Libby P. An HMG-CoA reductase inhibitor, cerivastatin, suppresses growth of macrophages expressing matrix metalloproteinases and tissue factor in vivo and in vitro. *Circulation*. 2001;103:276–283.
15. Liao JK. Effects of statins on 3-hydroxy-3-methylglutaryl coenzyme A reductase inhibition beyond low-density lipoprotein cholesterol. *Am J Card*. 2005;96:24F–33F.
16. Bea F, Blessing E, Bennett B, Levitz M, Wallace EP, Rosenfeld ME. Simvastatin promotes atherosclerotic plaque stability in apoE-deficient mice independently of lipid lowering. *Arterioscler Thromb Vasc Biol*. 2002;22:1832–1837.
17. Johnson J, Carson K, Williams H, Karanam S, Newby A, Angelini G, George S, Jackson C. Plaque rupture after short periods of fat feeding in the apolipoprotein E-knockout mouse: model characterization and effects of pravastatin treatment. *Circulation*. 2005;111:1422–1430.
18. Ni W, Egashira K, Kataoka C, Kitamoto S, Koyanagi M, Inoue S, Takeshita A. Antiinflammatory and antiarteriosclerotic actions of HMG-CoA reductase inhibitors in a rat model of chronic inhibition of nitric oxide synthesis. *Circ Res*. 2001;89:415–421.
19. Egashira K, Hirooka Y, Kai H, Sugimachi M, Suzuki S, Inou T, Takeshita A. Reduction in serum cholesterol with pravastatin improves endothelium-dependent coronary vasomotion in patients with hypercholesterolemia. *Circulation*. 1994;89:2519–2524.
20. Takemoto M, Liao JK. Pleiotropic effects of 3-hydroxy-3-methylglutaryl coenzyme a reductase inhibitors. *Arterioscler Thromb Vasc Biol*. 2001;21:1712–1719.
21. Egashira K. Clinical importance of endothelial function in arteriosclerosis and ischemic heart disease. *Circ J*. 2002;66:529–533.
22. Kubo M, Egashira K, Inoue T, Koga J, Oda S, Chen L, Nakano K, Matoba T, Kawashima Y, Hara K, Tsujimoto H, Sueishi K, Tominaga R, Sunagawa K. Therapeutic neovascularization by nanotechnology-mediated cell-selective delivery of pitavastatin into the vascular endothelium. *Arterioscler Thromb Vasc Biol*. 2009;29:796–801.
23. Oda S, Nagahama R, Nakano K, Matoba T, Kubo M, Sunagawa K, Tominaga R, Egashira K. Nanoparticle-mediated endothelial cell-selective delivery of pitavastatin induces functional collateral arteries (therapeutic arteriogenesis) in a rabbit model of chronic hind limb ischemia. *J Vasc Surg*. 2010;52:412–420.
24. Chen L, Nakano K, Kimura S, Matoba T, Iwata E, Miyagawa M, Tsujimoto H, Nagaoka K, Kishimoto J, Sunagawa K, Egashira K. Nanoparticle-mediated delivery of pitavastatin into lungs ameliorates the development and induces regression of monocrotaline-induced pulmonary artery hypertension. *Hypertension*. 2011;57:343–350.
25. Gibaud S, Demoy M, Andreux JP, Weingarten C, Gouritin B, Couvreur P. Cells involved in the capture of nanoparticles in hematopoietic organs. *J Pharm Sci*. 1996;85:944–950.
26. Sigovan M, Boussel L, Sulaiman A, Sappey-Marinier D, Alsaid H, Desbleds-Mansard C, Ibarrola D, Gamondès D, Corot C, Lancelot E, Raynaud JS, Vives V, Laclédère C, Violas X, Douek PC, Canet-Soulas E. Rapid-clearance iron nanoparticles for inflammation imaging of atherosclerotic plaque: initial experience in animal model. *Radiology*. 2009;252:401–409.
27. Ishibashi M, Egashira K, Zhao Q, Hiasa K, Ohtani K, Ihara Y, Charo IF, Kura S, Tsuzuki T, Takeshita A, Sunagawa K. Bone marrow-derived monocyte chemoattractant protein-1 receptor CCR2 is critical in angiotensin II-induced acceleration of atherosclerosis and aneurysm formation in hypercholesterolemic mice. *Arterioscler Thromb Vasc Biol*. 2004;24:e174–e178.
28. Satoh K, Nigro P, Matoba T, O'Dell MR, Cui Z, Shi X, Mohan A, Yan C, Abe J, Illig KA, Berk BC. Cyclophilin A enhances vascular oxidative stress and the development of angiotensin II-induced aortic aneurysms. *Nat Med*. 2009;15:649–656.
29. Ishibashi M, Hiasa K, Zhao Q, Inoue S, Ohtani K, Kitamoto S, Tsuchihashi M, Sugaya T, Charo IF, Kura S, Tsuzuki T, Ishibashi T, Takeshita A, Egashira K. Critical role of monocyte chemoattractant protein-1 receptor CCR2 on monocytes in hypertension-induced vascular inflammation and remodeling. *Circ Res*. 2004;94:1203–1210.
30. Han KH, Ryu J, Hong KH, Ko J, Pak YK, Kim JB, Park SW, Kim JJ. HMG-CoA reductase inhibition reduces monocyte CC chemokine receptor 2 expression and monocyte chemoattractant protein-1-mediated monocyte recruitment in vivo. *Circulation*. 2005;111:1439–1447.
31. Swirski FK, Libby P, Aikawa E, Alcaide P, Luscinskas FW, Weissleder R, Pittet MJ. Ly-6C^{hi} monocytes dominate hypercholesterolemia-associated monocytosis and give rise to macrophages in atheromata. *J Clin Invest*. 2007;117:195–205.
32. Nahrendorf M, Swirski FK, Aikawa E, Stangenberg L, Wurdinger T, Figueiredo JL, Libby P, Weissleder R, Pittet MJ. The healing myocardium sequentially mobilizes two monocyte subsets with divergent and complementary functions. *J Exp Med*. 2007;204:3037–3047.
33. Gough PJ, Gomez IG, Wille PT, Raines EW. Macrophage expression of active MMP-9 induces acute plaque disruption in apoE-deficient mice. *J Clin Invest*. 2006;116:59–69.
34. Ni W, Egashira K, Kitamoto S, Kataoka C, Koyanagi M, Inoue S, Imaizumi K, Akiyama C, Nishida KI, Takeshita A. New anti-monocyte chemoattractant protein-1 gene therapy attenuates atherosclerosis in apolipoprotein E-knockout mice. *Circulation*. 2001;103:2096–2101.
35. Inoue S, Egashira K, Ni W, Kitamoto S, Usui M, Otani K, Ishibashi M, Hiasa K, Nishida K, Takeshita A. Anti-monocyte chemoattractant protein-1 gene therapy limits progression and destabilization of established atherosclerosis in apolipoprotein E-knockout mice. *Circulation*. 2002;106:2700–2706.
36. Ni W, Kitamoto S, Ishibashi M, Usui M, Inoue S, Hiasa K, Zhao Q, Nishida K, Takeshita A, Egashira K. Monocyte chemoattractant protein-1 is an essential inflammatory mediator in angiotensin II-induced progression of established atherosclerosis in hypercholesterolemic mice. *Arterioscler Thromb Vasc Biol*. 2004;24:534–539.
37. Matoba T, Egashira K. Anti-inflammatory gene therapy for cardiovascular disease. *Curr Gene Ther*. 2011;11:442–446.
38. Rosenfeld ME, Polinsky P, Virmani R, Kauser K, Rubanyi G, Schwartz SM. Advanced atherosclerotic lesions in the innominate artery of the ApoE knockout mouse. *Arterioscler Thromb Vasc Biol*. 2000;20:2587–2592.
39. Clarke MC, Figg N, Maguire JJ, Davenport AP, Goddard M, Littlewood TD, Bennett MR. Apoptosis of vascular smooth muscle cells induces features of plaque vulnerability in atherosclerosis. *Nat Med*. 2006;12:1075–1080.
40. Robbins CS, Hilgendorf I, Weber GF, Theurl I, Iwamoto Y, Figueiredo JL, Gorbatov R, Sukhova GK, Gerhardt LM, Smyth D, Zavitz CC, Shikatani EA, Parsons M, van Rooijen N, Lin HY, Husain M, Libby P, Nahrendorf M, Weissleder R, Swirski FK. Local proliferation dominates lesional macrophage accumulation in atherosclerosis. *Nat Med*. 2013;19:1166–1172.
41. Koga J, Egashira K, Matoba T, Kubo M, Ihara Y, Iwai M, Horiuchi M, Sunagawa K. Essential role of angiotensin II type 1a receptors in the host vascular wall, but not the bone marrow, in the pathogenesis of angiotensin II-induced atherosclerosis. *Hypertens Res*. 2008;31:1791–1800.
42. Mantovani A, Garlanda C, Locati M. Macrophage diversity and polarization in atherosclerosis: a question of balance. *Arterioscler Thromb Vasc Biol*. 2009;29:1419–1423.
43. Robbins CS, Chudnovskiy A, Rauch PJ, Figueiredo JL, Iwamoto Y, Gorbatov R, Etzrodt M, Weber GF, Ueno T, van Rooijen N, Mulligan-Kehoe MJ, Libby P, Nahrendorf M, Pittet MJ, Weissleder R, Swirski FK. Extramedullary hematopoiesis generates Ly-6C(high) monocytes that infiltrate atherosclerotic lesions. *Circulation*. 2012;125:364–374.

44. Wong B, Lumma WC, Smith AM, Sisko JT, Wright SD, Cai TQ. Statins suppress THP-1 cell migration and secretion of matrix metalloproteinase 9 by inhibiting geranylgeranylation. *J Leukoc Biol.* 2001;69:959–962.
45. Worthylake RA, Lemoine S, Watson JM, Burridge K. RhoA is required for monocyte tail retraction during transendothelial migration. *J Cell Biol.* 2001;154:147–160.
46. Sata M, Nishimatsu H, Osuga J, Tanaka K, Ishizaka N, Ishibashi S, Hirata Y, Nagai R. Statins augment collateral growth in response to ischemia but they do not promote cancer and atherosclerosis. *Hypertension.* 2004;43:1214–1220.
47. Matoba T, Sato K, Egashira K. Mouse models of plaque rupture. *Curr Opin Lipidol.* 2013;24:419–425.

CLINICAL PERSPECTIVE

Acute myocardial infarction is the most severe type of coronary heart disease. Recent advances in therapeutic intervention for acute myocardial infarction have been associated with an increased prevalence of heart failure with high long-term mortality, which remains a serious concern worldwide. The pathophysiological process of acute myocardial infarction includes atherosclerotic coronary plaque destabilization and rupture. In clinical settings, the use of HMG-CoA reductase inhibitors (statins) reduces cardiovascular risks; however, even a high-dose strong statin is insufficient to suppress acute myocardial infarction. In the present study, we identified circulating $CCR2^{+}Ly\text{-}6C^{high}$ inflammatory monocytes/macrophages as a culprit and a therapeutic target for plaque destabilization and rupture. We engineered poly(lactic-co-glycolic acid) (PLGA) nanoparticles containing pitavastatin, which was taken up mainly by circulating monocytes. PLGA nanoparticle–mediated delivery of pitavastatin inhibited aortic atherosclerosis and the plaque destabilization and rupture associated with decreased monocyte chemoattractant protein-1/CCR2 signaling–mediated monocyte infiltration and gelatinase activity in the plaque. A nanoparticle-mediated drug-delivery system potentiates the therapeutic efficacy of pitavastatin at least 20-fold compared with daily oral administration of pitavastatin. We are now performing a phase I/IIa clinical trial of nanoparticles encapsulated with pitavastatin in patients with critical limb ischemia (UMIN [University Hospital Medical Information Network] clinical trial registry No. UMIN000008011). Given the safety profile of GMP (good manufacturing practices)-compliant pitavastatin-encapsulated nanoparticles, future clinical trials will examine their clinical value in patients with unstable coronary plaques. Finally, nanoparticle-mediated drug delivery is a novel modality that may advance current statin treatment for unstable plaques and achieve an optimal therapeutic strategy for the prevention of acute myocardial infarction in the future.

SUPPLEMENTARY MATERIAL

Supplementary Materials and Methods

Diet preparation

A high-fat diet (HFD) that contained 21% fat from lard and was supplemented with 0.15% (wt/wt) pure cholesterol (Oriental yeast, Tokyo Japan) was prepared according to the formula recommended by the American Institute of Nutrition. This diet contained the following constituents: casein, cystine, corn starch, sucrose, cholic acid, a mineral mixture, a vitamin mixture, powdered cellulose, choline bitartrate, and tert-butylhydroquinone.

Experimental protocols

At 16 to 18 weeks of age, mice began receiving the HFD. After 4 weeks of HFD, all mice were infused with angiotensin II dissolved in phosphate-buffered saline (PBS) at 1.9 mg/kg per day via an osmotic mini-pump (Alzet, Cupertino, CA, USA) for 4 weeks.[1, 2] Systolic blood pressure and heart rate were measured by the tail-cuff method and body weight was measured 4 weeks after the angiotensin II infusion. Mice were euthanized with intraperitoneal injection of pentobarbital at day 28 of angiotensin II infusion for analysis. Blood samples were collected via the left ventricles. Commercially available enzyme-linked immunosorbent assay kits (Wako Pure Chemical Industries, Osaka, Japan) were used to measure plasma lipid profiles (total cholesterol and triglycerides). Serum levels of various biomarkers were measured with the Luminex LabMAP instruments (Charles River Laboratories, Wilmington, MA, USA) (http://www.criver.com/en-US/ProdServ/ByType/Discovery/Pages/PlasmaBiomarkerAnalysis.aspx).

Experimental protocol 1: To examine whether inflammation-activated macrophages accelerate plaque destabilization and rupture, $CCR2^{+/+}$-inflammatory macrophages from the peritoneal cavity of $ApoE^{-/-}CCR2^{+/+}$ mice and $CCR2^{-/-}$-leukocytes from the peritoneal

cavity of $ApoE^{-/-}CCR2^{-/-}$ mice were collected three days after intraperitoneal injection of 2 ml of 0.05% thioglycollate (BD Biosciences, Franklin Lakes, NJ, USA), and these cells were directly injected intravenously three times during angiotensin II infusion. At the beginning of the angiotensin II infusion, animals were divided into 2 groups: (i) the $CCR2^{+/+}$-inflammatory macrophage group ($1x10^6$ cells/ 200 μl PBS) (n=5); and (ii) the $CCR2^{-/-}$-leukocyte group ($1x10^6$ cells/ 200 μl PBS) (n=8). Mice were euthanized over a several day period after 4 weeks of angiotensin II infusion for this protocol.

Experimental protocol 2: To examine the effect of nanoparticle-mediated delivery of pitavastatin on plaque destabilization and rupture, animals were divided into 4 groups at the beginning of angiotensin II infusion: (i) the no treatment group (n=9); (ii) the FITC-incorporated NP group (0.1 mg PLGA/ 200 μl PBS) (n=7); (iii) the pitavastatin-only group (0.012 mg pitavastatin/ 200 μl PBS) (n=6); and (iv) the pitavastatin-incorporated NP group (0.1 mg PLGA/ 0.012 mg pitavastatin/ 200 μl PBS) (n=10). FITC-NP, pitavastatin, and pitavastatin-NP were administered intravenously via the tail vein once per week.

Experimental protocol 3: To examine the effect of nanoparticle-mediated delivery of the 7ND plasmid (a dominant negative inhibitor of MCP-1^{3-6}) on plaque destabilization and rupture, animals were divided into 2 groups at the beginning of the angiotensin II infusion: (i) the FITC-incorporated NP group (1.3 mg PLGA/ 200 μl PBS) (n=12); and (ii) the 7ND plasmid-incorporated NP group (1.3 mg PLGA/ 5 μg 7ND plasmid/ 200 μl PBS) (n=10). NPs were administered by weekly intravenous injection.

Experimental Protocol 4: To examine the effect of daily oral administration of pitavastatin on plaque destabilization and rupture, animals were divided into 2 groups at the beginning of angiotensin II infusion: (i) the low pitavastatin group (lower dose: 0.1 mg/kg per day); and (ii) the high pitavastatin group (higher dose: 1.0 mg/kg per day). Pitavastatin was

administered by oral gavage every day for 4 weeks.

The no treatment group in protocol 2 was also used as the control group in protocols 1 and 4.

Histopathology

To quantify the extent of the atherosclerotic lesions in the whole aorta, the aortic arch and the thoracic aorta was opened longitudinally, stained with oil red O, and pinned on a black wax surface. The percentage of the plaque area stained by oil red O with respect to the total luminal surface area was quantified. To quantify the extent of the atherosclerotic lesions in the aortic root, approximately 3 serial cross sections (5 μm thick) of the aortic root were prepared according to the method described by Paigen et al,[7] with a slight modification. In brief, atherosclerotic lesions in the aortic sinus region were examined at 3 locations, each separated by 100 μm, with the most proximal site starting after the appearance of at least two aortic valve leaflets. Serial sections were stained with elastica van Gieson (EVG). The largest plaque of the three valve leaflets was adopted for morphological analysis. The brachiocephalic arteries were embedded in paraffin or OCT compound (Sakura Finetechnical Co. Ltd, Tokyo, Japan). Sections were cut at 3 μm for paraffin-embedded sections or 5 μm for OCT-embedded sections. Three sets of serial sections obtained at 30 μm intervals (starting from the proximal end) were stained with EVG to measure the total number of disrupted and buried fibrous caps, as previously described.[8] Disrupted and buried fibrous caps were defined as follows. A disrupted fibrous cap was defined as a visible defect in the cap accompanied by an intrusion of erythrocytes into the plaque. A buried fibrous cap was defined as an elastin layer that was overlaid with foam cells. All morphometric analyses were made on EVG-stained sections, and three vessel cross sections were quantified per mouse by computerized image analysis. Fibrous cap thickness was determined at the thinnest part of the cap by computerized image

analysis. The analysis was necessarily restricted to those plaques that had developed sufficiently to form fibrous caps, and the average thickness of three fibrous caps per section was obtained for quantitative analysis. Plaque macrophage or MCP-1 expression areas were determined by the ratio of Mac3- or MCP-1-positive areas to the intima areas of plaques.

Immunohistochemistry

Serial brachiocephalic arterial sections adjacent to those sections that were stained with EVG were deparaffinized, and endogenous peroxidase was blocked by incubation with 0.3% H_2O_2 in methanol for 5 minutes. For antigen retrieval, sections were boiled for 20 minutes in citrate buffer (pH=6.0). After blocking with 3% skim milk, sections were incubated overnight at 4°C with the following antibodies: anti-mouse macrophage antibody (Mac3; dilution 1:100, Santa Cruz Biotechnology Inc., Santa Cruz, CA, USA), and anti-mouse MCP-1 antibody (dilution 1:200, Santa Cruz Biotechnology Inc., Santa Cruz, CA, USA) followed by incubation with biotin-conjugated secondary antibodies. Then, the sections were washed and treated with avidin-peroxidase. The sections were developed using the DAB substrate kit (Wako Pure Chemical Industries, Osaka, Japan), and nuclei were counterstained with hematoxylin. Serial aortic root sections were also stained using anti-mouse Mac3 antibody. Multiple observers who were blinded to the experiment protocol performed the quantitative analysis. All images were captured with a Nikon microscope equipped with a digital camera (HC-2500) and analyzed using Adobe Photoshop 6.0 (Adobe Systems, San Jose, CA, USA) and Scion Image 1.62 for Windows (Scion, Frederick, MD, USA).

Flow cytometry

Peripheral blood was drawn via a cardiac puncture, and red blood cells were lysed with

VersaLyse Lysing solution (Becton Dickinson Biosciences, San Jose, California) for 10 minutes at room temperature. Spleens were removed and triturated in HBSS at 4 °C and filtered through nylon mesh (BD Biosciences). The cell suspension was centrifuged at 300 x *g* for 5 minutes at 4 °C. Red blood cells were also lysed with VersaLyse Lysing solution. After blocking the Fc receptor with anti-CD16/32 mAb (BD Pharmingen, San Diego, California) for 5 minutes at 4°C, peripheral leukocytes were incubated with a cocktail of CA, USA against CD11b-APC (BD Pharmingen, San Diego, California), CD115-PE (BD Pharmingen, San Diego, California) and Ly-6C-FITC (eBioscience, San Diego, CA, USA), and peritoneal leukocytes were incubated with a cocktail of mAb against F4/80-APC (AbD Serotec, Oxford, UK), CD115-PE (BD Pharmingen) and Ly-6C-FITC (eBioscience) for 30 minutes at 4°C; all leukocytes were then analyzed with FACSCalibur (Becton Dickinson Biosciences, San Jose, CA, USA). For the cellular uptake of FITC-NPs, leukocytes were incubated with a cocktail of mAb against lineage cell marker (Lin: CD90/B220/CD49b/NK1.1/Ly-6G)-PE (BD Pharmingen, San Diego, CA, USA) and CD11b-APC. The leukocytes were also incubated with appropriate isotype controls (BD Pharmingen, San Diego, CA, USA). Macrophage subsets were identified as either Ly-6C^{hi}F4/80^{+}CD115^{+} or Ly-6C^{lo}F4/80^{+}CD115^{+}, as previously described.[9] Monocyte subsets were identified as either Ly-6C^{hi}CD11b^{+}CD115^{+} or Ly-6C^{lo}CD11b^{+}CD115^{+}, as previously described.[10] For the cellular uptake of FITC-NPs, neutrophils and monocytes were identified as Lin^{+}CD11b^{+} and Lin^{-}CD11b^{+}, respectively.

In vivo accumulation of inflammation-activated macrophages

Thioglycollate-elicited macrophages were labeled with PKH26 (Sigma Aldrich, St. Louis, MO, USA) *ex vivo* according to the manufacturer's protocol. 24 hours after the intravenous injection of PKH26-labeled macrophages, the brachiocephalic arteries were

fixed with 3.7% formaldehyde and embedded in OCT compound. Sections were cut at 5 μm for OCT-embedded sections and evaluated by fluorescence microscopy. Nuclei were stained with DAPI (Vector Laboratories Inc., Burlingame, California).

Splenic Monocyte/Macrophage isolation and adoptive transfer

Splenic monocytes and macrophages were obtained by negative selection using the Mouse Monocytes Enrichment Kit (StemCell Technologies, British Columbia, Canada) according to the manufacturer's protocol. In brief, monocytes and macrophages were isolated from an $ApoE^{-/-}$ mouse spleen. Cells were passed through a 100 μm nylon filter, and suspended in lysis buffer. Mouse monocytic cells were further purified from the spleens using the Purple EasySep magnet (StemCell Technologies) prior to flow cytometry analysis. These cells (0.8-1.0 $x10^6$ cells/ 200 μl PBS) were directly injected intravenously via the femoral vein once to $ApoE^{-/-}$ mice fed a high-fat diet and infused with angiotensin II. Mice were euthanized with intraperitoneal injection of pentobarbital at day 7 of angiotensin II infusion for analysis.

Preparation of PLGA nanoparticles

Poly(lactic-co-glycolic acid) (PLGA) polymer with an average molecular weight of 20,000 and a lactide-to-glycolide copolymer ratio of 75:25 (Wako Pure Chemical Industries, Osaka, Japan) was used to prepare the nanoparticles. PLGA nanoparticles incorporated with fluorescein isothiocyanate (FITC; Dojindo Laboratories, Kumamoto, Japan) (FITC-NP), pitavastatin (Kowa Pharmaceutical Co Ltd, Tokyo, Japan) (pitavastatin-NP), or 7ND plasmid (7ND-NP) were prepared by a previously reported emulsion solvent diffusion method in purified water.[11-13] PLGA was dissolved in a mixture of acetone and methanol. Then, FITC, pitavastatin, or 7ND plasmid was added to this solution. The resultant PLGA-FITC, PLGA-pitavastatin, or PLGA-7ND solution was

emulsified in polyvinyl alcohol with stirring at 400 rpm using a propeller-type agitator with 3 blades (Heidon 600G, Shinto Scientific, Tokyo, Japan). After the system was agitated for 2 hours under reduced pressure at 40°C, the entire suspension was centrifuged (20,000 x *g* for 20 minutes at -20°C). After the supernatant was removed, purified water was added and mixed with the sediment. The wet mixture was then centrifuged again to remove excess polyvinyl alcohol and the unencapsulated reagent that could not adsorb onto the surfaces of the nanoparticles. After this process was repeated, the resultant dispersion was freeze-dried under the same conditions. The FITC-, pitavastatin-, or 7ND-loaded PLGA nanoparticles contained 5.0% (w/v) FITC, 12.0% (w/v) pitavastatin, or 0.40% (w/v) 7ND, respectively. The average diameters of the PLGA-NPs were 231 nm, 159 nm, and 290 nm for the FITC-NP, pitavastatin-NP, and 7ND-NP, respectively. The surface charges (zeta potential) analyzed by Zetasizer Nano (Sysmex, Hyogo, Japan) were -16.7 mV, -4 mV, and 8.1 mV, respectively.

Cellular uptake and in vitro kinetics of the nanoparticles

Murine peritoneal macrophages were obtained from wild-type mice that were injected intraperitoneally with 2 ml of 0.05% thioglycollate 72 hours before the extraction. The cells were centrifuged at 1,000 rpm for 5 minutes at 4°C, suspended in lysis buffer and washed twice with phosphate-buffered saline (PBS) for 5 minutes at 4°C. The cell pellets were suspended in DMEM plus 10% FBS and 1% PS at an initial concentration of 5.0×10^5 cells/ml in a 35 mm culture dish. FITC-NPs were added to the dish (1.0 mg PLGA/ml) and incubated at 37°C in a 5% CO_2 environment overnight. After two washes with PBS for 5 minutes at room temperature, the cells were fixed with methanol and counterstained with propidium iodide (Vector Laboratories Inc., Burlingame, CA, USA). The intracellular uptake of FITC-NP was evaluated by fluorescence microscopy (BX50,

Olympus, Tokyo, Japan) and confocal microscopy (FV1000-D, Olympus). RAW264.7, a murine macrophage cell line, was purchased from the American Type Culture Collection (ATCC; Manassas, VA, USA). The cells were seeded on 6-well-chamber slides and incubated at 37°C in a 5% CO_2 environment until they were subconfluent. The growth medium was replaced with 2 ml of an OsO_4-NP suspension medium (1.0 mg PLGA/ml), incubated for 6 hours and fixed with 2.5% glutaraldehyde. The intracellular uptake of OsO_4-NPs was observed by transmission electronic microscopy (Hitachi H7000E, Tokyo, Japan). To examine the FITC kinetics of cultured macrophages, confluent RAW264.7 cells were incubated with FITC-NP or FITC only at the indicated concentrations (1, 3, 10, 30, and 100 μM). After 2 hours of incubation, extracellular FITC-NPs or FITC was washed out, and FITC with diffuse interference contrast image was observed by confocal laser microscopy (Nikon A1R, Tokyo, Japan) at the indicated time points (days 0, 1, 4, and 7). The average fluorescent intensity of FITC was analyzed using the National Institutes of Health Image Software.

In vivo kinetics of the nanoparticles

The whole aortas of $ApoE^{-/-}$ mice that were fed with HFD and infused with angiotensin II were excised 24 hours after an intravenous injection of the FITC-NPs. The excised aortas were evaluated by stereoscopic and fluorescence microscopy (Nikon SMZ1500 equipped with Nikon HB-10103AF and appropriate fluorescence filter sets, Tokyo, Japan). The brachiocephalic arteries were fixed with 3.7% formaldehyde and embedded in OCT compound. Sections were cut at lengths of 5 μm and evaluated by fluorescence microscopy (BX50, Olympus). The nuclei were stained with propidium iodide (Vector Laboratories Inc., Burlingame, CA, USA). Serial sections were stained with hematoxylin-eosin.

In situ zymography

Gelatinase (MMP-2/gelatinase-A and MMP-9/gelatinase-B) activity was measured in unfixed frozen sections (6 μm thick) using quenched fluorescein-labeled gelatinase substrate (DQ gelatin, Invitrogen, Eugene, OR, USA).[14] The fluorescent area produced by the proteolytic digestion of quenched fluorescein-labeled gelatin was recognized as combined gelatinase activity (MMP-2 + MMP-9). The brachiocephalic artery sections were incubated at 37°C for 30 minutes according to the manufacturer's protocol. Fluorescent microscopy was used to detect gelatinase activity as green fluorescence. Negative control zymograms were incubated in the presence of 20 mM EDTA. The specific removal of essential divalent cations resulted in no detectable gelatinolytic activity.

Gelatin zymography

The RAW264.7 cells were prepared as described above. The growth medium was replaced with pitavastatin at 0.01, 0.1, or 1 μM; pitavastatin-incorporated NPs containing 0.0367, 0.367, or 3.67 μg/mL of PLGA and 0.01, 0.1, or 1 μM of pitavastatin; FITC-incorporated NPs containing 3.67 μg/mL of PLGA-NP; or the vehicle alone. When the medium was replaced, LPS was added at 25 ng/mL to each well. Twenty-four hours after the LPS stimulation, the culture supernatant was obtained. The supernatant was subjected to gelatin zymography using the Gelatin Zymo-Electrophoresis Kit (Primary Cell, Hokkaido, Japan) according to the manufacturer's directions.

Real-time quantitative RT PCR

Real-time PCR amplification was performed with the mouse cDNA with the use of the ABI PRISM 7000 Sequence Detection System (Applied Biosystems), as described previously.[15] For mouse MCP-1, the sense and antisense PCR primers were

5'-CCTGGATCGGA-ACCAAATGA-3' and 5'-CGGGTCAACTTCA-CATTCAAAG-3', respectively, and the probe oligonucleotide was 5'-AACT-GCATCTGCCCTAAGG-TCTTCAGCA-3'. For mouse CCR2, the sense and antisense primers were 5'-CCTTGGGA-ATGAGTAACTGTGTGAT-3' and 5'-ATGGA-GAGATACCTTCGGAACTTCT-3', and the probe oligonucleotide was 5'-CACTTAGACCAGGCCATGCAGGT-GACA-3'. The GAPDH probe was purchased from Applied Biosystems.

Chemotaxis assay

THP-1, the human monocyte cell line, was obtained from the German Collection of Micro-organisms and Cell Cultures (DSMZ; Brauschweig, Germany). The cells were cultured in RPMI 1640 with 10% FBS and 37°C in a 5% CO_2 environment until they were subconfluent. The growth medium was replaced with starvation medium with pitavastatin-NPs containing 0.00367 to 36.7 μg/mL of PLGA and 0.001 to 10 μM of pitavastatin, FITC-NPs containing 36.7 μg/mL of PLGA, or vehicle alone for 24 hours. The chemotactic activity of THP-1 cells in response to 10 ng/mL MCP-1 was measured in a 96-well microchemotaxis Boyden chamber (ChemoTx; Neuroprobe), as described previously.[16] Monocytes that had transmigrated through the micropore were stained with trypan blue. The number of monocytes that migrated in response to MCP-1 was counted.

Measurements of statin concentration in plasma

Pitavastatin concentrations in plasma were measured at predetermined time points by liquid chromatography coupled to tandem mass spectrometry (LC/MS/MS). Briefly, the high-performance liquid chromatography (HPLC) analysis was performed using Agilent 1100 series system (Agilent Technologies, Inc, Santa Clara, CA, USA). The column temperature was maintained at 40 °C. The flow rate was 0.3 mL/min. Pre-prepared plasma

solutions were injected from the autosampler into the HPLC system. The turbo ion spray interface was operated in the positive ion mode at 4800 V and 550 °C. The analytical data were processed using Analyst software (version 1.4, Applied Biosystems, Foster City, CA, USA).